

Article

Laser Welding of BTi-6431S High Temperature Titanium Alloy

Zhi Zeng ^{1,*}, J. P. Oliveira ², Xianzheng Bu ³, Mao Yang ¹, Ruoxi Li ⁴ and Zhimin Wang ^{3,*}

¹ School of Mechatronics Engineering, University of Electronic Science and Technology of China, Chengdu 611731, China; 201521080159@std.uestc.edu.cn

² Department of Materials Science and Engineering, The Ohio State University, Columbus, OH 43221, USA; jp.oliveira@campus.fct.unl.pt

³ Beijing Hangxing Machinery Manufacture Limited Corporation, Beijing 100013, China; nirubu@163.com

⁴ College of Materials Science and Engineering, Beijing University of Technology, Beijing 100124, China; liruoxi_0927@126.com

* Correspondence: zhizeng@uestc.edu.cn (Z.Z.); d201677150@hust.edu.cn (Z.W.); Tel.: +86-028-6183-0229 (Z.Z.); +86-010-8810-3289 (Z.W.)

Received: 27 September 2017; Accepted: 13 November 2017; Published: 15 November 2017

Abstract: A new type of high temperature titanium alloy, BTi-6431S, has recently become the focus of attention as a potential material for aircraft engine applications, which could be used up to 700 °C. Pulsed laser welding was used to butt join the BTi-6431S titanium alloy in order to understand the feasibility of using fusion-based welding techniques on this material. The effect of laser energy on the microstructure and mechanical properties of the joints was investigated. The microstructural features of the joints were characterized by means of microscopy and X-ray diffraction. Tensile testing was conducted at both room temperature and high temperature to simulate potential service conditions. The results show that the microstructure of the laser welded joints consists of primary α phase and needle α' phase, while the microstructure of the heat affected zone consists of α , β , and needle α' phases. The tensile strength of the welded joints at room temperature was similar to that of the base material, despite a reduction in the maximum elongation was observed. This was related to the unfavorable microstructure in the welded joints. Nonetheless, based on these results, it is suggested that laser welding is a promising joining technique for the new BTi-6431S titanium alloy for aerospace applications.

Keywords: high temperature titanium alloy; laser welding; microstructure; mechanical properties; BTi-6431S

1. Introduction

Titanium alloys are widely used in the aerospace field to manufacture important structures which are used at high temperatures and/or under complex stress states, due to unarguable properties such as excellent corrosion resistance, high specific mechanical resistance, and excellent high temperature performance [1,2]. However, with the development of high performance flying technology, more strict requirements are put forward for the performance of titanium alloys in the aerospace field [3]. The need for improved fatigue resistance, mass reduction, and corrosion resistance in the aircraft industry has raised interest in using titanium alloys with higher specific strength to replace stainless steels and other high temperature alloys in some structural and mechanical parts [4,5].

Many studies have been performed to investigate the welding performance of titanium alloys. It is reported that tungsten inert gas (TIG) welding of Ti-6Al-4V alloy plates resulted in the highest impact strength as compared to laser and electron beam welding [6]. Gao et al. [7] found that for welding thin sheets of titanium alloys, TIG welding led to higher residual distortions and a coarse microstructure. Laser welding

can be considerably adaptable for joining titanium alloys in large size and complex structures. Such a joining technique has recently been increasing in popularity as one of the preferred welding methods for most critical titanium components in the aerospace industry [8,9]. Nd:YAG pulsed laser beam welding is an advanced joining process in which melting and solidification of the weld zone takes place after each pulse by a more dense heat source [10]. Squillace et al. investigated the conduction and keyhole regime based on heat input range of Nd:YAG laser beam welding and concluded that weld morphology was highly dependent on the welding regime [11]. Campanelli et al. [12] studied the effect of laser welding parameters on Ti6Al4V alloy and found out that the tensile strength of the joints was of 80% of that of the base material, with fracture occurring in a brittle way, suggesting the need for a post-weld heat treatment to be applied on the welds. Shen et al. [13] applied laser beam welding to weld dissimilar titanium alloys, and the effect of laser beam offset on microstructural characterizations and mechanical properties of the joints were investigated. If proper welding procedures are found to effectively join titanium alloys so that the joint achieves the desired properties, it can also result in the efficient utilization of materials and save on expenditure.

In general, welding of Ti alloys can be associated with some metallurgical problems. For example, in TIG welding Ti6246 alloys, the elongation of the weld metal is reported to be of only 0.4% [14]. This weld brittleness is related to the formation of brittle phases, precipitation of hard and brittle particles, and formation of hydrides in the weld metal [11,13,15]. Similarly, in laser welded Ti-6Al-4V, an $\alpha + \beta$ titanium alloy, it is reported that the hardness in the weld zone is 140 HV higher than that of the base material [16]. This increase in the weld hardness is related to the formation of secondary martensite due to the high cooling rates upon weld metal solidification [9,11]. Similar metallurgical problems are experienced when performing dissimilar welding of Ti-based alloys to other materials [17].

Recently, a new type of Ti-Al-Sn-Zr-Mo-Nb-W-Si series high temperature titanium alloy, named BTi-6431S, has become the focus of attention as a potential material for aircraft engine applications which could be used up to 700 °C [18]. It can meet the current high-speed aircraft demand for harsh working conditions, with broad application prospects. Until now, there has only been limited research on the microstructure, mechanical properties, and superplastic forming technology of the BTi-6431S alloy, with reports on the welding performance of this titanium alloy being scarce [13,18,19]. In this study, the effect of laser welding on the high temperature titanium alloy BTi-6431S was investigated. The microstructure and mechanical properties of the laser welded joint were analyzed and tested, providing a theoretical basis and experimental data for its application in future aircraft structures.

2. Materials and Experiments

The BTi-6431S titanium alloy sheets utilized for the laser welding were 200 mm × 100 mm × 2.2 mm. The chemical composition of the base material is listed in Table 1, in weight percentage. Prior to welding, the oxide film on the surface of each work piece was removed using a specific acid solution (4 mL hydrofluoric acid, 10 mL nitric acid, and 86 mL distilled water). The specimens were cleaned with acetone and ethanol, and subsequently dried.

Table 1. Chemical composition of BTi-6431S high temperature titanium alloy (wt %).

Ti	C	Si	Mo	N	O	Zr	Nb	Sn	W	Al	H	Fe
Bal.	0.0077	<0.1	1.26	0.0039	0.068	2.94	1.12	3.21	0.47	6.28	0.0052	0.018

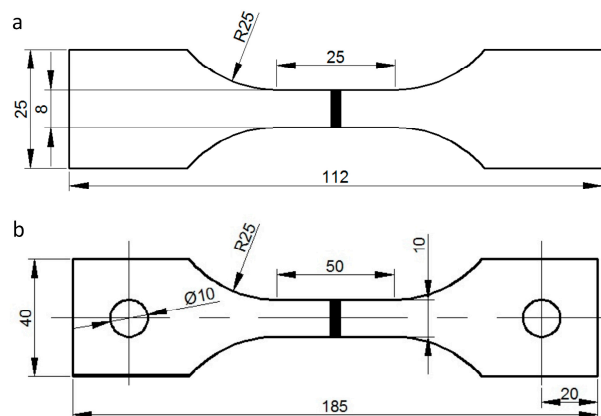
Welding was performed using a Trumpf HL 4006D laser (TRUMPF Co. Ltd., Ditzingen, Germany) with a wavelength of 1.064 nm. The welding parameters used to perform similar butt joining of the BTi-6431S titanium alloy are depicted in Table 2.

Table 2. Laser welding parameters used to join the BTi-6431S titanium alloy.

Welding Parameters	
Base power (W)	850
Peak power (W)	1600
Pulse duration (ms)	20
Duty ratio (%)	50
Welding speed (mm/min)	1500
Focal length (mm)	120
Focal position (mm)	0
Spot diameter (μm)	400

After welding, cross sections of the joints were prepared for metallographic observation. The microstructural characterization was performed by optical microscopy using an Olympus PMG3 (Olympus Corporation, Tokyo, Japan). X-ray diffraction (XRD) was performed to determine the phases present in the base material and weld regions using a Philips XRD system (Royal Dutch Philips Electronics Ltd., Amsterdam, The Netherlands) operating at 40 kV and 30 mA equipped with a Cu source, which is used as line 0.05° of step size in 2θ and 2 s/step. To examine the variation in the chemical composition across the weld, electron microprobe analysis (EPMA) was performed on the as-polished samples using a JEOL 733 SuperProbe (JEOL Ltd., Tokyo, Japan) operating at 10 kV and 50 nA. A micro-hardness profile across the weld beads of the welded coupons was obtained using a Leco[®] Microhardness Tester LM248AT (LECO Corporation, Saint Joseph, MO, USA). All the hardness readings were obtained using a load of 500 g with a dwell time of 15 s.

Wire electrodischarge machining (WEDM), abrasive waterjet (AWJ), or laser cutting could be alternative processes to conventional milling to produce tensile test specimens. These processes have the advantage of being extensively used in the sheet metal forming industry, whose effect on tensile strength were lower than 5% [20]. For mechanical characterization of the welded joints, dog-bone shaped specimens were prepared after WEDM (6 mm/min, 0.18 mm Mo wire, $V_d = 80$ V, $I = 3$ A) with dimensions depicted in Figure 1. Tensile tests were performed at room temperature and at 650°C following the ASTM E8-13a standard. A 30 kN Instron 5582 universal tensile testing machine (Instron Corporation, Norwood, MA, USA) using a travel speed of 2 mm/min was used. The tensile testing direction was perpendicular to the weld interface and the welded region was located in the center of the dog-bone specimens. The maximum stress and strain of the samples were recorded. The base material was also tested at both room and high temperature for comparison of the effect of laser welding on the mechanical properties. Following the tensile experiments, the fracture surfaces of the specimens were investigated by scanning electron microscope (SEM) using a Zeiss Supra 55 SEM (Zeiss Group, Heidenheim, Germany).

**Figure 1.** Dimensions of the dog-bone specimens used for tensile testing: (a) sample design for room temperature testing; (b) sample design for high temperature testing. (Unit: mm).

3. Appearance of Welded Joints

3.1. Appearance of Welded Joints

Figure 2a,b exhibits the appearance of the face and root of the welded joints. It can be observed that the bead formations were uniform with a bright silver color, which indicates that the surfaces of the weld were not contaminated by oxygen, nitrogen, or carbon. However, the surfaces of the joints were slightly concave and misaligned as observed in Figure 2c.

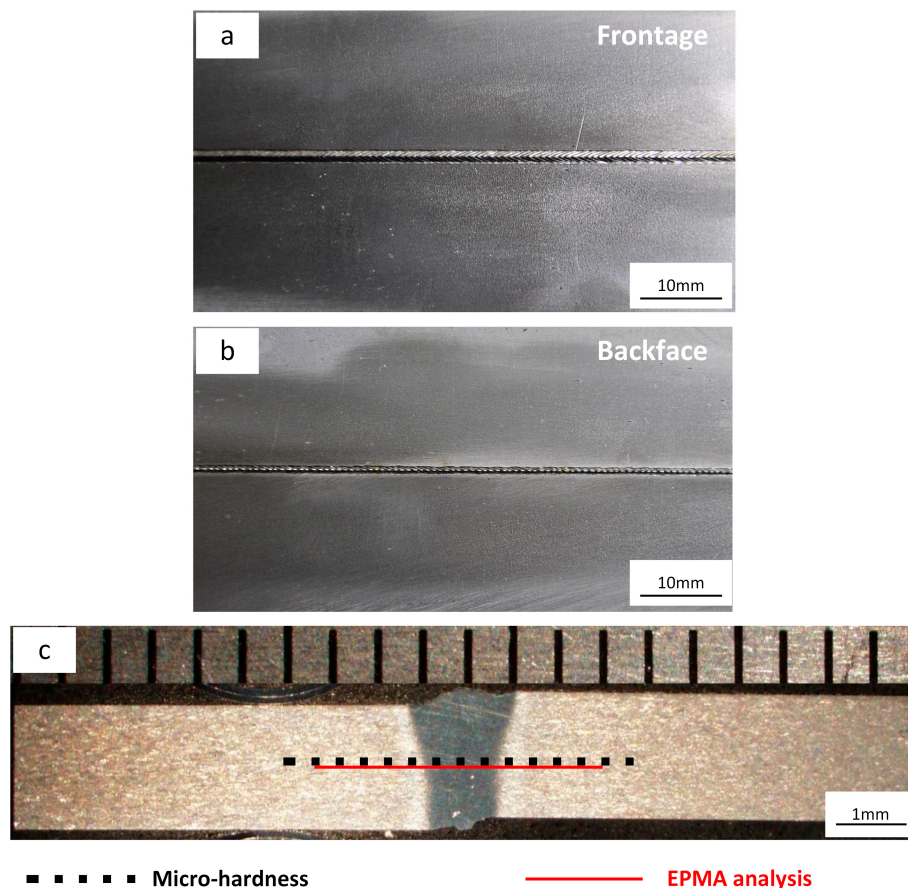


Figure 2. Appearance of BTi-6431S laser welding joint: (a) face of the welded joint; (b) root of the welded joint; (c) macro view of the surface of weld with indication of the location of the microhardness and EPMA testing.

3.2. Microstructural Characterization

The microstructure of the BTi-6431S titanium alloy base material consisted of the β phase which was distributed at the elongated α grain boundaries (shown in Figure 3). This microstructure resulted in the dislocation plug product in the phase boundaries, which could improve the materials toughness, creep resistance, and creep rupture strength at high temperatures, especially for aircraft engine application [21].

The overall morphology of the laser welded joints can be depicted in Figure 4a. The laser welded joint consisted of four zones, which were weld zone (WZ), high temperature heat effect zone (H-HAZ), low temperature heat effect (L-HAZ), and base material (BM).

Some pores were identified in the fusion zone of the welded joint. Several factors may explain the presence of pores: keyhole instability, pre-existence of pores in the base material and poor shielding conditions [22,23]. The weld zone was a typical basket weave pattern (Figure 4b). A large amount of

primary acicular structures was uniformly distributed in the α -phase substrate. It has been illustrated that the main phase present in the weld zone was the α phase, as identified by XRD analysis (Figure 4c).

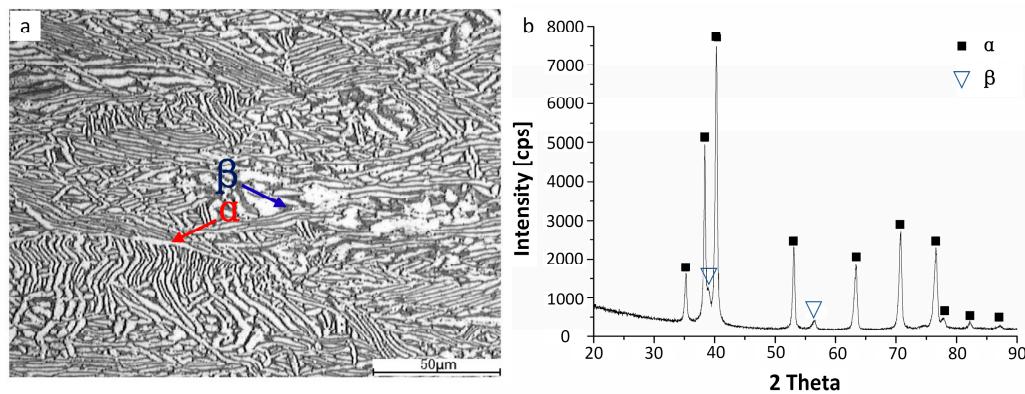


Figure 3. Microstructure and phase composition of base metal: (a) optical microscopy; (b) X-ray diffraction pattern.

The microstructural transformations of the welded joint primarily depends on the initial microstructure of the base metal and the temperature cycle experienced during the welding process. The key aspects of the temperature cycle include the heating rate, maximum heating temperature, the dwelling time at high temperature, and the cooling rate [24]. During the welding process, the liquid metal within the weld initially crystallized to form the β phase. During the subsequent cooling process, owing to the rapid cooling rate, part of the β phase could not transform into the α phase through atomic diffusion, and it mainly transformed into α' martensite via shear transformation. The shear transformation mode depends on the regular short-range migration of the atoms in the β phase [25]. For titanium-based alloys [26–28], the starting and finish temperatures of the martensite transformation depends on the chemical composition of the alloy. In general, as the amount of the β stabilizer elements increases, there is a greater resistance for the phase transition required for lattice reconfiguration. Therefore, a higher degree of supercooling was required for the phase transformation, and the martensite start transition temperature reduced. Additionally, for Ti-based alloys, diffusion-controlled transformations are favored for slow cooling rates, whereas high cooling rates as those found in laser welding favor the shear transformation [29]. As such, part of the β phase transformed into the α' phase. Zhang et al. [30] demonstrated that the β phase stabilizer elements did not only enrich the β phase but also reduced the amount of α' martensite. As shown in Figure 4c, the XRD results demonstrated that only the diffraction peaks corresponding to the α phase could be observed. As both α' martensite and acicular α exhibited a hexagonal structure and their lattice constants were similar, there was a superimposition of the diffraction peaks of both the α and α' phases, thus preventing identification of both phases through this technique.

As the distance from the boundary of the fusion zone increased, the maximum temperature and cooling rate decreased. The distinct HAZ microstructural features are mainly due to the different weld thermal cycles. The optical micrograph in Figure 4a demonstrates that the grain size increased in the high temperature heat affected zone (H-HAZ) towards the low temperature heat affected zone (L-HAZ) and that the microstructure mainly consisted of acicular α and martensite α' in the H-HAZ. This was mainly because the peak heating temperature is assumed to be higher than the β transition temperature and that the α phase completely transformed into the β phase during the welding process [13]. During the subsequent cooling process, the β phase transformed into acicular α and martensite α' as a result of the rapid cooling rate. However, the cooling rate was still slower than that of the WZ and the amount of martensite α' in the H-HAZ was less than that in the WZ.

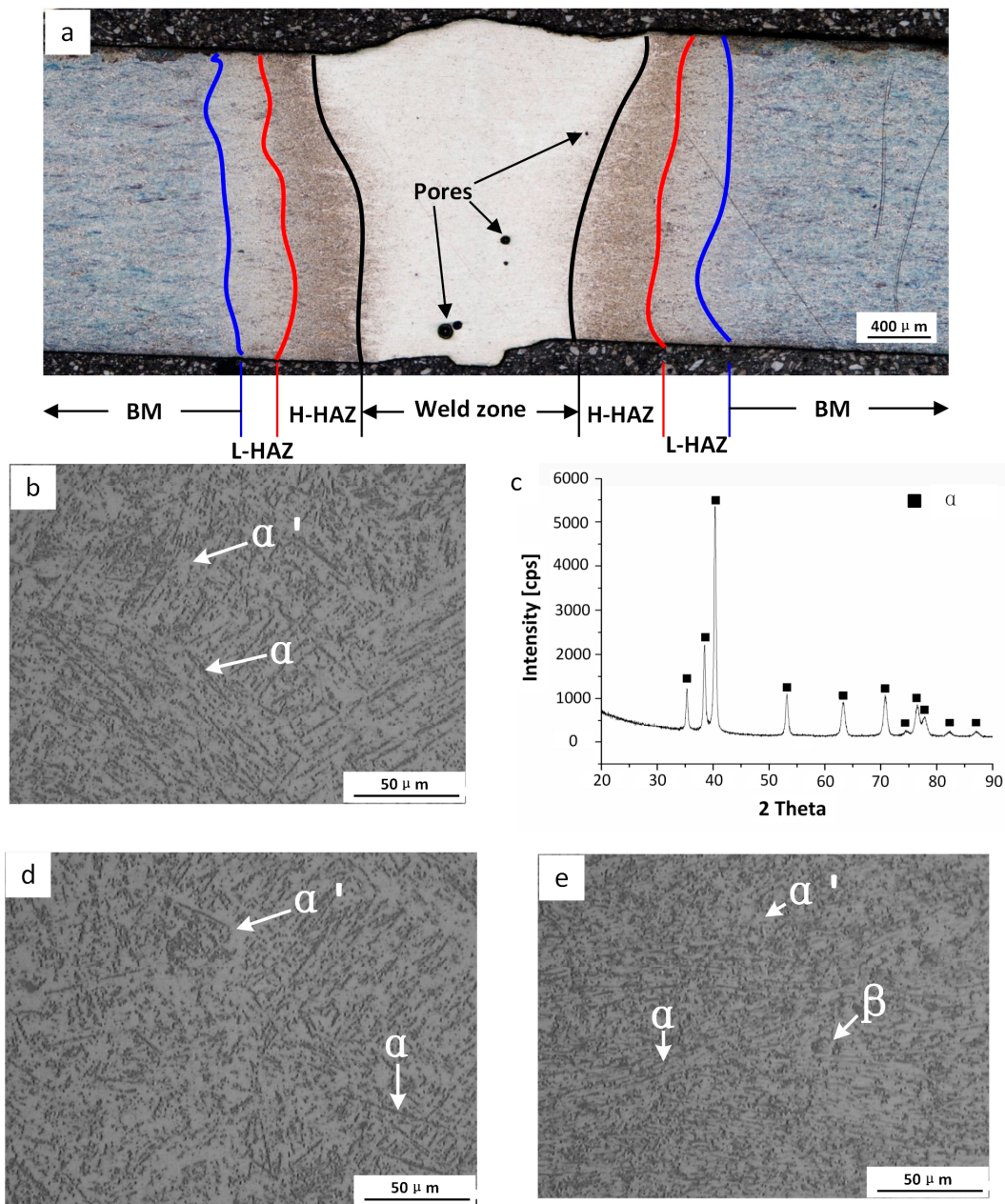


Figure 4. Macro and microstructure of joint and X-ray diffraction pattern: (a) macrostructure; (b) microstructure of the welded region; (c) X-ray diffraction pattern of the welded region; (d) microstructure of high temperature heat affected zone; (e) microstructure of low temperature heat affected zone.

The L-HAZ extends from a position where the weld thermal cycle has no observable effect on the original microstructure to a position where the temperature is lower than the β transition temperature. The microstructure of the L-HAZ differed from the microstructure adjacent to the fusion line where the temperature was above the β phase transition temperature (H-HAZ). Figure 4e showed that the microstructure in the L-HAZ mainly consisted of a mixture of secondary α' , primary α , and prior β phase. In the L-HAZ, as the distance between the base metal and the fusion line decreased, the prior β phase gradually transformed into the secondary α' phase. This was mainly because of the peak heating temperature, which is assumed to be lower than the β transition temperature and that the temperature of the L-HAZ reached the zone of the α and β phase transition temperature [31,32]. As the temperature in the L-HAZ was not high enough and the retention time was not long enough, the microstructure

consisted of α and β phase under a high temperature and there was still a significant amount of primary α phase retained. In the subsequent cooling process, transformation of the α phase did not occur, and the secondary α phase formed at the grain boundaries and grain interiors of the β phase. Thus, the microstructure of the L-HAZ exhibited a mixture of secondary α' , primary α , and prior β phase. The temperature increases as the distance from the fusion line decreases. Therefore, the closer to the fusion line, the more prior β phase would transfer into the secondary α' phase during the subsequent cooling process.

The chemical composition variation along the welded joint of major alloying elements in the fusion zone of BTi-6431S, determined by EPMA, are presented in Figure 5. It can be observed that the distribution of Al, Nb, Sn, Zr, and Mo from the fusion zone to the base material does not change significantly. This is a sign of a sound weld since losing alloying elements during welding in the fusion zone due to evaporation is not desirable due to possible detrimental effects on the mechanical properties of the joint. For Al, Nb, Zr, and Mo there are slight fluctuations (about 8%) in the distribution of these alloying elements in the L-HAZ and BM regions. This can be explained in terms of the presence of α and β phases in both the L-HAZ and BM. Indeed, due to a small testing zone (about 5 μm) and coarser α and β sizes, depending on whether the measurement location was on α or β phase, a different chemical composition was measured as these alloying elements have different affinities for α and β phases [33].

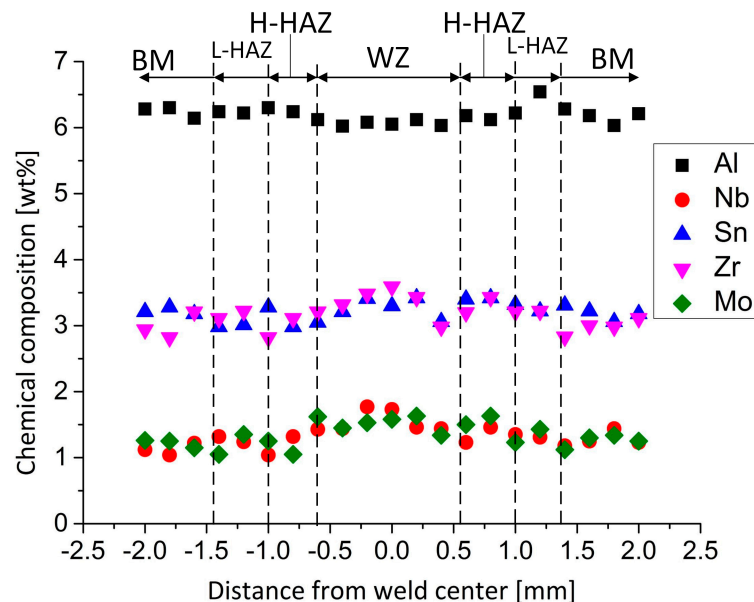


Figure 5. Chemical composition of BTi-6431S laser weld joint.

3.3. Mechanical Properties of the Joints

In order to map the variation in the mechanical properties across the weld, microhardness measurements were performed. The variation in the microhardness across the material is plotted in Figure 6. It can be seen that by moving from the BM toward the L-HAZ and H-HAZ the hardness increases in the welded specimen. For the BM, the hardness varies from 351 to 364 HV. This small variation can be related to the indent size and α/β size. The average indent diameter was 24 μm while α and β had the respective size of $32.5 \pm 15.3 \mu\text{m}$ and $12.7 \pm 5.3 \mu\text{m}$ as determined by digital image analysis taking as reference the microstructure of the base material depicted in Figure 3a. Therefore, hardness can be measured either mostly on the β phase, or partly on α and partly on β . Since β is softer and more ductile than α , there will be some variation in the measured hardness of the base material. In contrast, in the weld zone the microstructure was uniform which increased the hardness values to $412 \pm 4 \text{ HV}$ with α and secondary α' phases as previously presented. Additionally, an increased amount of harder acicular martensite α resulted in a significantly higher hardness than the BM. In the

WZ, it is noted that a small kink in the hardness peak leading two micro-hardness peaks was observed. Also, the variation in the hardness in along the WZ is not significant. In the H-HAZ, closer to WZ, more martensite α' is formed due to a higher peak temperature. The increasing amount of α' from the base material/heat affected zone interface towards the fusion boundary justifies the increasing hardness observed in Figure 6. Almost a symmetric hardness profile was observed for the two sides of the weld centerline. The observed symmetry in the microhardness profiles with respect to the weld centerline indicates that the two weld parts are affected thermally almost in the same way.

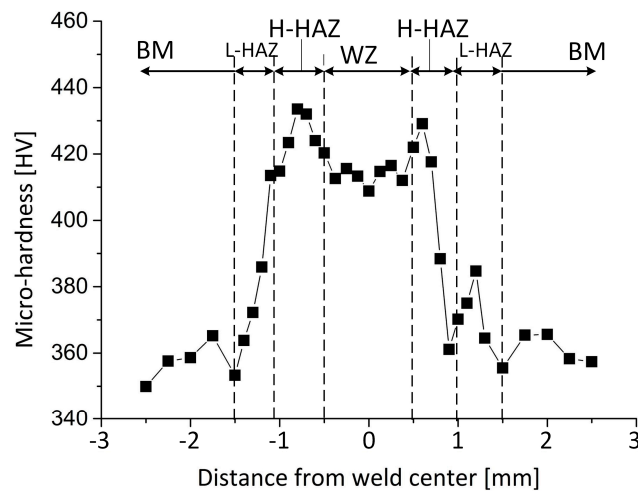


Figure 6. Microhardness profile along the cross section of the laser welded joint.

A summary of the results of the tensile tests conducted at room temperature for welded specimens and base material are depicted in Table 3. The tensile strength for the welds was determined from three dog-bone tensile samples extracted from the laser welded sheet. At room temperature, the average ultimate tensile strength (UTS) was 1050 MPa, the average elongation was 4.9% and the yield strength (YS) is 993 MPa. One must be aware that the tensile properties of a given sample specimen may be dependent on the methodology used to obtain it, as described in the literature [20,34,35]. However, since the same process was used for all test specimens any potential detrimental effect is diluted within the test itself.

Fracture of the welded joint occurred in the heat affected zone. Compared to the base material, the tensile strength is nearly the same, while the elongation is decreased significantly. According to [36], the strength of the existing phases demonstrates the following order: $\alpha' > \alpha > \beta$. Additionally, α' possesses very high hardness and low ductility and toughness [37]. The microstructure of the fusion zone consisted of martensite α' and a slender acicular α phase, whereas the microstructure of the heat affected zone consisted of acicular α phase, α' martensite, and β phase. The combination of coarse grain size, presence of α' martensite, and sharp hardness variation promoted fracture in the heat affected zone of the joints. The equiaxed morphology of the grains in the base material in terms of its mechanical properties is better than the microstructure which composes the heat affected and fusion zones. The present of coarse grain structures and phases with very distinct mechanical properties, may cause localized deformation during tensile testing and therefore premature rupture in one of these regions may occur. When the sample is tensile loaded, the dislocations are able to pile up between the α and β phases, which could prevent the micro-cracks initiation-extension and present better toughness than the welds [38]. The tensile results were consistent with the microstructural distribution of the welded joints, and it suggested that the post-weld heat treatment (PWHT) can improve the mechanical properties in brittle Ti alloy welds [18]. Additionally, it was reported that when welding Ti-Al alloys as the one used in this investigation, careful control of the welding parameters is necessary to obtain a sound joint [39,40].

Table 3. Summary of the mechanical testing performed on the welded specimens and base material at room temperature (RT) and 650 °C. For the base material the average results presented are based on a total of three samples tested at both temperatures.

Mechanical Testing Summary	Sample Reference	Temperature (°C)	UTS (MPa)	YS (MPa)	Elongation (%)	Fracture Location
Welded specimens	W1	RT	1072	988	5.1	HAZ
	W2	RT	1040	1002	4.8	HAZ
	W3	RT	1045	991	5.0	HAZ
	W4	650	776	683	4.4	HAZ
	W5	650	755	672	4.2	HAZ
	W6	650	765	681	4.5	HAZ
Base material	BM1	RT	1060 ± 15	982 ± 13	16.5 ± 0.3	-
	BM2	650	890 ± 17	824 ± 16	13.2 ± 0.5	-

When the tensile tests were performed at 650 °C, the yield strength and tensile strength drastically decreases to approximately 679 MPa and 765 MPa (about 82% and 86% of that of the base material at the same testing temperature), respectively. However, no significant reduction in the elongation of the welded joints tested at room and high temperature was observed. It should be noted, however, that the BTi-6431S laser weld could still support significant loads at high temperature, which is of significant importance for aircraft engine design using this new material. Similar to what was observed on the room temperature tensile tests, all the welded specimens fractured in the heat affected zone with evidence of necking and it could be observed that the surfaces were oriented at 45° from the tensile axis.

Figure 7 depicts the fracture surfaces of the welded specimens in the tensile testing at room temperature and 650 °C. The fracture surfaces demonstrated that the failure was mixed mode combining brittle and ductile features for the samples tested at room temperature. It was observed from the SEM analysis that the fracture surface tends to be mainly intergranular, and there are still some small and shallow dimples (ranging between 5 and 10 µm in size) which were shown in Figure 7c. Some of the pores that were observed in the microstructural observation performed using optical microscopy can also be observed in the fracture surface of the welded joint.

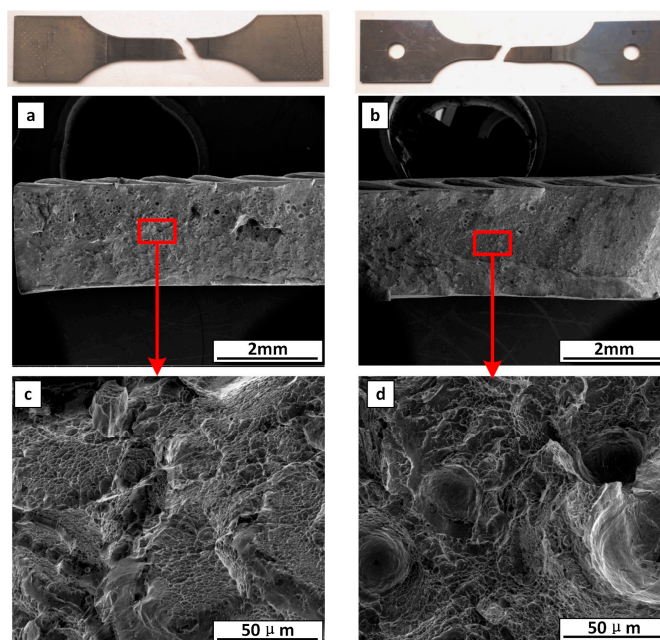


Figure 7. Fracture surface of welded joints: (a) fracture surface after tensile test performed at room temperature; (b) fracture surface after tensile test performed at 650 °C; (c) high magnification of the red box in (a); (d) high magnification of the red box in (b).

4. Conclusions

The quality of the laser welded BTi-6431S titanium alloy sheet in terms of tensile properties, microhardness, chemical composition distribution, and microstructure in the as-welded condition was investigated. The following conclusion can be drawn:

1. The base material microstructure of the BTi-6431S high temperature titanium alloy consisted of long strip and equiaxed α phases, with a small amount of β phase distributed between the α phase. The welded region was composed of primary α phase and a significant amount of acicular α' phase, showing basket weave pattern which resulted from the high degree of supercooling during the laser welding process. The microstructure in heat affected zone contained primary α phase, a small amount of β phase, and acicular α' phase.
2. The microhardness values of the weld zone and heat affected zone were higher than that of base metal. This was due to the fast cooling rate during the laser welding process, resulting in a large amount of α' martensitic phase distributed in the weld zone and the heat affected zone near the fusion line.
3. In this experiment, the tensile strength of the welded joint at room temperature was basically equivalent to the base metal due to the high strength phase distribution and nearly unchanged chemical composition. The tensile strength at high temperature decreased to about 765 MPa which tends to be mainly cleavage fracture with some dimples. The plasticity of the joint was obviously lower than that of the parent metal, and the elongation was about 5%. This was related to the formation of α' martensite in both the heat affected and fusion zone. All the specimens fractured in the heat affected zone with evidence of necking and it could be observed that the surfaces were oriented at 45° with the tensile axis.

Acknowledgments: Zhi Zeng acknowledge Science and Technology Planning Project of Guangdong Province (Grant No. 2016A010102002) and the Fundamental Research Funds for the Central Universities (Grant No. ZYGX2015J149).

Author Contributions: Zhi Zeng and Zhimin Wang conceived and designed the experiments; Xianzheng Bu performed the experiments; Ruoxi Li analyzed the data; Mao Yang contributed materials/analysis tools; Zhi Zeng and J. P. Oliveira wrote the paper.

Conflicts of Interest: The authors declare no conflict of interest.

References

1. Schwab, H.; Palm, F.; Kuhn, U.; Eckert, J. Microstructure and mechanical properties of the near-beta titanium alloy Ti-5553 processed by selective laser melting. *Mater. Des.* **2016**, *105*, 75–80. [[CrossRef](#)]
2. Zeng, Z.; Wu, X.; Yang, M.; Peng, B. Welding distortion prediction in 5A06 aluminum alloy complex structure via inherent strain method. *Metals* **2016**, *6*, 214. [[CrossRef](#)]
3. Babu, N.K.; Sundara Raman, S.G.; Murthy, C.V.S.; Reddy, G.M. Effect of beam oscillation on fatigue life of Ti-6Al-4V electron beam weldments. *Mater. Sci. Eng. A* **2017**, *471*, 113–119. [[CrossRef](#)]
4. Peters, M.; Kumpfert, J.; Ward, C.H.; Leyens, C. Titanium alloys for aerospace applications. *Adv. Eng. Mater.* **2010**, *5*, 419–427. [[CrossRef](#)]
5. Lu, K. The future of metals. *Science* **2010**, *328*, 319–320. [[CrossRef](#)] [[PubMed](#)]
6. Balasubramanian, T.S.; Balakrishnan, M.; Balasubramanian, V.; Manickam, M.A.M. Influence of welding processes on microstructure, tensile and impact properties of Ti-6Al-4V alloy joints. *Chin. J. Nonferrous Met.* **2011**, *21*, 1253–1262. [[CrossRef](#)]
7. Gao, X.L.; Zhang, L.J.; Liu, J.; Zhang, J.X. A comparative study of pulsed Nd:YAG laser welding and TIG welding of thin Ti6Al4V titanium alloy plate. *Mater. Sci. Eng. A* **2013**, *559*, 14–21. [[CrossRef](#)]
8. Lei, Z.L.; Dong, Z.J.; Chen, Y.B.; Huang, L.; Zhu, R.C. Microstructure and mechanical properties of laser welded Ti-22Al-27Nb/TC4 dissimilar alloys. *Mater. Sci. Eng. A* **2013**, *559*, 909–916. [[CrossRef](#)]
9. Winco, K.C.; Yung, B.R.; Leec, W.B.; Fenn, R. An investigation into welding parameters affecting the tensile properties of titanium welds. *J. Mater. Proc. Technol.* **1997**, *63*, 759–764.

10. Ghaini, F.M.; Hamed, M.J.; Torkamany, M.J.; Sabbaghzadeh, J. Weld metal microstructural characteristics in pulsed Nd:YAG laser welding. *Scr. Mater.* **2007**, *56*, 955–958.
11. Squillace, A.; Prisco, U.; Ciliberto, S.; Astarita, A. Effect of welding parameters on morphology and mechanical properties of Ti-6Al-4V laser beam welded butt joints. *J. Mater. Proc. Technol.* **2012**, *212*, 427–436. [[CrossRef](#)]
12. Campanelli, S.L.; Casalino, G.; Mortello, M.; Angelastro, A.; Ludovico, A.D. Microstructural characteristics and mechanical properties of Ti6Al4V alloy fiber laser welds. *Procedia CIRP* **2015**, *33*, 429–434. [[CrossRef](#)]
13. Zhang, H.; Hu, S.; Shen, J.; Li, D.; Bu, X. Effect of laser beam offset on microstructure and mechanical properties of pulsed laser welded BTi-6431S/TA15 dissimilar titanium alloys. *Opt. Laser Technol.* **2015**, *74*, 158–166. [[CrossRef](#)]
14. Mullins, F.D.; Becker, D.W. Property-microstructure relationships in metastable-beta titanium alloy Weldments. *Weld. Res. Suppl.* **1980**, *6*, 177–182.
15. Sabol, J.C.; Marvel, C.J.; Watanabe, M.; Pasang, T.; Misiolek, W.Z. Confirmation of the ω -phase in electron beam welded Ti-5Al-5V-5Mo-3Cr by high-resolution scanning transmission electron microscopy: An initial investigation into its effects on embrittlement. *Scr. Mater.* **2014**, *92*, 15–18. [[CrossRef](#)]
16. Akman, E.; Demir, A.; Canel, T.; Sinmazcelik, T. Laser welding of Ti6Al4V titanium alloys. *J. Mater. Proc. Technol.* **2009**, *209*, 3705–3713. [[CrossRef](#)]
17. Oliveira, J.P.; Miranda, R.M.; Fernandes, F.M.B. Welding and joining of NiTi shape memory alloys: A review. *Prog. Mater. Sci.* **2017**, *88*, 412–466. [[CrossRef](#)]
18. Zhang, W.J.; Song, X.Y.; Hui, S.X.; Ye, W.J.; Wang, Y.L. Effect of single annealing on microstructure and mechanical properties of BTi-6431S titanium alloy. *Chin. J. Nonferrous Met.* **2013**, *23*, 1530–1535.
19. Wang, X.X.; Wang, W.Q.; Ma, H.H. Microstructure and mechanical properties of high temperature and high strength BTi-6431S alloy at 700 °C. *Chin. J. Nonferrous Met.* **2010**, *20*, 792–795.
20. Krahmer, D.M.; Polvorosa, R.; de Lacalle, L.N.L.; Alonso-Pinillos, U.; Abate, G.; Riu, F. Alternatives for specimen manufacturing in tensile testing of steel plates. *Exp. Tech.* **2016**, *40*, 1555–1565. [[CrossRef](#)]
21. Casavola, C.; Pappalettere, C.; Pluvinage, G. Fatigue resistance of titanium laser and hybrid welded joints. *Mater. Des.* **2011**, *32*, 3127–3135. [[CrossRef](#)]
22. Zhao, H.; Debroy, T. Pore formation during laser beam welding of die-cast magnesium alloy AM60B-mechanism and remedy. *Weld. J.* **2001**, *80*, 204–210.
23. Zeng, Z.; Panton, B.; Oliveira, J.P.; Han, A.; Zhou, Y.N. Dissimilar laser welding of NiTi shape memory alloy and copper. *Smart Mater. Struct.* **2015**, *24*, 125036. [[CrossRef](#)]
24. Lee, J.Y.; Ko, S.H.; Farson, D.F.; Yoo, C.C. Mechanism of keyhole formation and stability in stationary laser welding. *J. Phys. D Appl. Phys.* **2002**, *35*, 1570–1576. [[CrossRef](#)]
25. Zhang, B.G.; Shi, M.X.; Chen, G.Q.; Feng, J.C. Microstructure and defect of titanium alloy electron beam deep penetration welded joint. *Chin. J. Nonferrous Met.* **2012**, *22*, 2633–2637. [[CrossRef](#)]
26. Deng, A.H. Martensitic transformation of titanium alloys. *Chin. J. Nonferrous Met.* **1999**, *20*, 193–199.
27. Thompson, S.A. An overview of nickel-titanium alloys used in dentistry. *Int. Endod. J.* **2000**, *33*, 297–310. [[CrossRef](#)] [[PubMed](#)]
28. Donachie, M.J. *Titanium: A Technical Guide*, 2nd ed.; ASM International: Novelt, OH, USA, 2000.
29. Threadgill, P.L. The prospects for joining titanium aluminides. *Mater. Sci. Eng. A* **1995**, *192*, 640–646. [[CrossRef](#)]
30. Zhang, H.T.; He, P.; Feng, J.C.; Wu, H.Q. Interfacial microstructure and strength of the dissimilar joint Ti 3 Al/TC4 welded by the electron beam process. *Mater. Sci. Eng. A* **2006**, *425*, 255–259. [[CrossRef](#)]
31. Liu, L.; Du, X.; Zhu, M.; Chen, G. Research on the microstructure and properties of weld repairs in TA15 titanium alloy. *Mater. Sci. Eng. A* **2007**, *445*, 691–696. [[CrossRef](#)]
32. Hsieh, C.T.; Chu, C.Y.; Shiue, R.K.; Tsay, L.W. The effect of post-weld heat treatment on the notched tensile fracture of Ti-6Al-4V to Ti-6Al-6V-2Sn dissimilar laser welds. *Mater. Des.* **2014**, *59*, 227–232. [[CrossRef](#)]
33. Junaid, M.; Baig, M.N.; Shamir, M.; Khan, F.N.; Rehman, K.; Haider, J. A comparative study of pulsed laser and pulsed TIG welding of Ti-5Al-2.5Sn titanium alloy sheet. *J. Mater. Proc. Technol.* **2017**, *242*, 24–38. [[CrossRef](#)]
34. Silva, C.M.; Rosa, P.A.; Martins, P.A. Innovative testing machines and methodologies for the mechanical characterization of materials. *Exp. Tech.* **2016**, *40*, 569–581. [[CrossRef](#)]

35. Han, Z.; Weatherley, D.; Puscasu, R. A relationship between tensile strength and loading stress governing the onset of mode I crack propagation obtained via numerical investigations using a bonded particle model. *Int. J. Num. Anal. Meth. Geomech.* **2017**, *1*–13. [[CrossRef](#)]
36. Lu, W.; Shi, Y.; Lei, Y.; Li, X. Effect of electron beam welding on the micro-structures and mechanical properties of thick TC4-DT alloy. *Mater. Des.* **2012**, *34*, 509–515. [[CrossRef](#)]
37. Sun, Z.; Annergren, I.; Pan, D.; Mai, T.A. Effect of laser surface remelting on the corrosion behavior of commercially pure titanium sheet. *Mater. Sci. Eng. A* **2003**, *345*, 293–300. [[CrossRef](#)]
38. Wang, Z.M.; Yao, W.; Shi, K. Research on laser welding and superplastic process for superalloy BTI-62421S. *Aeronaut. Manuf. Technol.* **2011**, *16*, 28–31.
39. Arenas, M.F.; Acoff, V.L. Analysis of Gamma titanium aluminide welds produced by gas tungsten arc welding. *Weld. J.* **2003**, *82*, 110–115.
40. Cao, J.; Qi, J.; Song, X.; Feng, J. Welding and joining of titanium aluminides. *Materials* **2014**, *7*, 4930–4962. [[CrossRef](#)] [[PubMed](#)]



© 2017 by the authors. Licensee MDPI, Basel, Switzerland. This article is an open access article distributed under the terms and conditions of the Creative Commons Attribution (CC BY) license (<http://creativecommons.org/licenses/by/4.0/>).